Indian Journal of Pure & Applied Physics
Vol. 60, October 2022, pp. 866-875
DOI: 10.56042/ijpap.v60i10.63614

On The Structure of Shock-Front in a Viscous and Heat Conducting Fluids

Anmol Singh* & R K Anand

Department of Physics, (UGC Centre of Advanced Studied) University of Allahabad, Prayagraj-211 002, India

Received 28 May 2022; accepted 15 September 2022

The internal structure of one-dimensional steady shock-front is investigated using the Navier-Stokes equations in a viscous and heat conducting gaseous medium. The analytical expression and calculations for the different flow variables *i.e*., the particle velocity, temperature, pressure, and change-in-entropy distribution have been derived using the method of wave-front analysis. The abrupt changes in the flow variables have been observed within the shock transition region. The thickness and inverse shock-front thickness are calculated and obtained results are compared with the reported literatures. The effects on the shock structure due to the variation of different flow parameters have been discussed in each case for all the flow variables. Obtained outcomes manifests that the flow parameters *i.e*., coefficient of viscosity, Mach number, adiabatic index and Prandtl number exert dominant impact on the structure of shock-front, prominently.

Keywords: Shock-front; Viscous and heat conducting fluids; Prandtl number; Entropy production

1 Introduction

In the field of shock waves, much advancement has been made in both theoretically and experimental regimes due to its wide applications[1-2] with respect to the structure of shock wave. The research is focused mainly on two problems. First one, its internal structure and other is the change in structure during its propagation. To better understand, it is important to know the internal structure of shock waves as well as their behavior during propagation in different media. Theoretical and experimental aspects have been studied on the internal structure of shock waves from time to time. In the theoretical point of view, finding solutions of the problems using the system of conservation laws have been broadly studied with lesser effort and it has attracted a lot of attention by the researcher. Theoretical models on the shock waves were first proposed by Rankine[3] and Hugoniot[4]. The study on the internal structure of shock-front plays a prominent role in understanding the various physical phenomena such as molecular dissociation, vibration excitations, radiation, *etc*., in high-energy physics.

To study the internal structure of the shock wave and the mechanism of the shock process, it is necessary to include the dissipation effect in the conservation laws. In many circumstances, it is appropriate to omit the heat conduction terms in the conservation laws. Since, the dissipative effects are produced by both viscosity and heat conduction. Therefore, both properties should be taken in the constitutive equations for a deeper analysis. Many works have been done on the structure of shock waves under different conditions and obtained analytical solution in viscous and thermal conductive mediums[5-9]. These works are a remarkable contribution to the preliminary study of shocks. A more generalized study was proliferated by Meyerhoff[10] and Puckett *et al*[11]. In 1950, Meyerhoff studied the structure of shock waves for weak and strong shock-fronts propagating in an ideal gas. On the other hand, Puckett *et al.* have given their idea in the context of structure of shock waves in air, which is more realistic assumption for gases. In addition, the pioneering works have been done by several authors[12-16] on the structure of the shock-front in a viscous and heat conducting medium with the help of compressible Navier-Stokes (N-S) equations for obtaining the analytical solutions in presence of dissipative processes. The internal structure of the shock wave-front in an ideal gas has been studied by many authors[17-20]. Experimental observations on the thickness of the shock-front for different gases were obtained by Elizarova *et al*[21].

More specifically, Zel'dovich *et al.*[22] studied the internal structure of a planar shock wave and gave an analytical model based on the Hugoniot curves for the

*Corresponding authors: (Email: anmolphy@rediffmail.com)

shock processes by taking into account the effect of viscosity and heat conduction. Thereafter, many authors[23-26] have studied internal structure of shock-front and explained the variation of flow variables within the shock transition region. Recently, a new scaling has been developed for the structure of shocks in an ideal gas[27]. Also, the researchers have developed a generalized method that can solve the non linear hydrodynamics equations for non linear compressible gas problems with high accuracy[28-29].

Initially, Morduc how and Libby obtained the thickness of shock-front with the help of N-S equations for a fixed Prandtl number in an ideal gas. Khidr *et al.*[30] explores the analytical solutions for arbitrary Prandtl numbers and high Mach numbers for a perfect gas. Later on, Johnson[31] derived a general solution for both large and small Prandtl numbers under constant viscosity and thermal conductivity. They have found a new technique to solve the problem of one-dimensional steady-state and constant viscosity equation of state at fixed Prandtl number. Recently, Patel and Singh obtained the exact solution of the shock wave structure under constant and variable coefficient of viscosity and thermal conductivity in a non-ideal gas for fixed and variable Prandtl number by continuum model and obtained results have been compared with different techniques[32,33].

The objective of the present study is to explore the internal structure of the shock-front using conservation equations in a viscous medium with heat conductivity. We have computed the exact analytical expression for the different flow variables. Subsequently, the thickness and reciprocal shock thickness was obtained using different flow parameters *viz.*, coefficient of viscosity, Mach number, adiabatic index, and Prandtl number within the shock transition region. Interestingly, our computations confirm that the effect on the flow variables such as particle velocity, temperature, pressure, and change-in-entropy distribution have reasonable impact on the structure of shock-front within the transition region. The effect of the flow parameters on the flow variables was shown graphically as well as the variations were tabulated in that region, and also results compared with previous study which was obtained from the different techniques. In our study, MATLAB code was used to make numerical computations in tables and graphs.

It is assumed that the gas is thermally perfect which means it obeys the ideal gas law $p = \rho R T$, where p, ρ, R are the pressure, density, and gas constant respectively. T is the absolute temperature of the gas. The relation between the thermal conductivity K and the Prandtl number P_r is correlated as[16], $K = \gamma R\mu/(\gamma-1)P_r$ where μ is the coefficient of viscosity, and γ is adiabatic exponent, which gives the ratio of specific heats of the gas. In general, the thermal conductivity lies between 0 and 1 for an ideal gas. The viscosity coefficient μ, which is a function of temperature and pressure, is examine to quantify the effect of viscous dissipation on the shock wave structure in gases. The present study is based upon to observe the effects of the different flow parameters including with coefficient of viscosity, Prandtl number, Mach number, adiabatic index *etc*., which are investigated on the flow variables. From these observations, the thickness of the shock-front depends significantly on the flow parameters.

2 The basic equations and boundary conditions

The Navier-Stokes Eulerian formulation for the one-dimensional by the principle of conservation equations of mass, momentum, and energy are

$$\frac{\partial \rho}{\partial t} + \rho \frac{\partial u}{\partial r} + u \frac{\partial \rho}{\partial r} = 0 \qquad ...(1)$$

$$\frac{\partial (\rho u)}{\partial t} + \frac{\partial (p + \rho u^2 - q)}{\partial r} = 0 \qquad ...(2)$$

$$\frac{\partial (\rho e + \rho u^2/2)}{\partial t} + \frac{\partial [\rho u (e + u^2/2) + pu - qu + Q]}{\partial r} = 0 \qquad ...(3)$$

where, the parameters $\rho(r,t)$, $u(r,t)$, $p(r,t)$, $q(r,t)$, $e(r,t)$ and $Q(r,t)$ are the density, particle velocity, pressure, viscous stress tensor, internal energy per unit mass and heat-flux respectively.The space coordinate r is the position with respect to origin in the direction normal to the shock-front and t is the time coordinates with respect to the shock-front. The viscous stress tensor is given by

$$q = \frac{4}{3}\mu \frac{du}{dr} \qquad ...(4)$$

From Fourier's Law of thermal conduction using the Navier-Stokes equations for the heat flow, the heat-flux can be expressed as[17]

$$Q = -K \frac{dT}{dr} \qquad ...(5)$$

where, K and T are the thermal conductivity and temperature of the gas respectively.

For further treatment to get exact solution of the flow variables in a gaseous phase flow medium, the equations of state are given as

$$p = \rho RT \quad ...(6)$$

$$e = p/\rho(\gamma - 1) = C_V T \quad ...(7)$$

where, $C_v = C_p - R$ .The specific heats C_p, C_v are the specific heat of the gas at constant pressure, volume and R denotes the gas constant. The used parameter 'e' defines the internal energy per unit mass. γ is ratio of specific heats of the gas.

The isentropic speed of sound denoted by a is given as

$$a = (\gamma p/\rho)^{1/2} \quad ...(8)$$

The thermal conductivity K is associated with the viscosity coefficient μ in terms of Prandtl number P_r can be expressed as[16, 17]

$$P_r = \mu C_p / K \quad ...(9)$$

The mean free path is given by[34,37]

$$\lambda_0 = \frac{\mu}{a_0 \rho_0 \sqrt{\pi\gamma/2}} = \mu\left(\sqrt{\pi/2\rho_0 p_0}\right) \quad ... (10)$$

where the parameter, a_0 is the speed of sound in the undisturbed medium.

Here, we have considered a coordinate system in which the shock-front is at rest and practically the shock strength remains unchanged within the small time interval (Δt) . It is notable that the time interval is of the order of the shock-front thickness. Thus, in the Navier-Stokes equations, the partial derivatives with respect to time $\left(\partial./\partial t\right)$ are neglected and the partial derivative with respect to space coordinate $(\partial./\partial r)$ is replaced by the total derivative $\left(d./dr\right)$. Now the Eq. (1-3) reduces to

$$u\frac{d\rho}{dr} + \rho\frac{du}{dr} = 0 \quad ...(11)$$

$$\frac{d(p + \rho u^2 - q)}{dr} = 0 \quad ...(12)$$

$$\frac{d[\rho u(e + u^2/2) + pu - qu + Q]}{dr} = 0 \quad ...(13)$$

To obtain the solutions of the set of differential Eq. (11-13) with the boundary condition

$$u_0 = U \quad ...(14)$$

where, u_0 is the initial particle velocity.

These solutions require that the gradients of the flow variables must vanish ahead of the shock-front $(r = +\infty)$ as well as behind the shock-front $(r = -\infty)$. The flow variables p_0, ρ_0, u_0 and p, ρ and U. The notation '0' stands for initial values *i.e.*, just ahead of the shock-front and without suffix denotes as final values of the flow variables use as just behind the shock-front.

2.1 Exact solutions for the flow variables

To find the exact solutions with flow variables, we integrate Eq. (11-13) with boundary condition Eq. (14), and some elementary operations, in the equilibrium state and then using Eq. (7), the shock profile equations can be written as

$$\rho = \rho_0 U/u \quad ...(15)$$

$$p = p_0 + q + \rho_0 U^2 - \rho u^2 \quad ...(16)$$

$$\rho u\left[p/\rho(\gamma - 1) + u^2/2\right] + pu - qu + Q = \rho_0 U\left[p_0/\rho_0(\gamma - 1) + U^2/2\right] + p_0 U \quad ...(17)$$

Solving Eq. (15) and Eq. (16) and putting them in Eq. (17), we get

$$\gamma p_0 u + qu + \gamma\rho_0 u U^2 - \rho\gamma u^3 + (\gamma - 1)\frac{\rho u^3}{2} - K(\gamma - 1)\frac{dT}{dr} = \gamma p_0 U + (\gamma - 1)\frac{\rho_0 U^3}{2} \quad ...(18)$$

To find the exact solutions for the flow variables, it is convenient to use the dimensionless quantities called particle velocity η and shock strength M are given as $\eta = u/U = \rho_0/\rho$ and $M = U/a_0$ (19)

where a_0 is the speed of sound in the unshocked medium, defined as $a_0 = (\gamma p_0/\rho_0)^{1/2}$.

Using Eq. (4, 5, 8, 9) and Eq. (19) substituting in Eq. (18) we get,

$$a_1\eta^2 + b_1\eta + c_1 = \eta g_1 \frac{d\eta}{dr} \quad ...(20)$$

where, $a_1 = (\gamma+1)/2$, $b_1 = -\left(1/M^2+\gamma\right)$

$c_1 = \left(1/M^2 + (\gamma-1)/2\right)$ and $g_1 = \frac{1}{M(\gamma p_0\rho_0)^{1/2}}\left[\frac{4\mu}{3} - \frac{\mu\gamma(\gamma-1)}{P_r}\right]$

From Eq. (20), quadratic with η and since in an equilibrium state, the flow variables do not contain the gradients, *i.e.*, the gradient of the flow variables must be vanishing ahead and behind of the shock-front. Thus, at this condition, the profile of particle velocity at maximum in that state is given by $d\eta/dr = 0$ with $\eta = \eta_{eq}$.

For, η_{eq} the two solutions of Eq. (20) are

$$\eta_{eq} = \left[-b_1 \pm \left(b_1^2 - 4a_1c_1\right)^{1/2}\right] \Big/ 2a_1 \quad ...(21)$$

Here, we designate the first equilibrium state by η_1 with the positive sign and another second equilibrium state with flow variables by η_2 with the negative sign as

$$\eta_{1,2} = \left[-b_1 \pm \left(b_1^2 - 4a_1c_1\right)^{1/2}\right] \Big/ 2a_1 \quad ...(22)$$

Integrating Eq. (20) using with Eq. (21) gets an expression for Particle velocity with distance *r* from the origin as

$$r = (g_1/a_1)\left[A\log(\eta-\eta_1) + B\log(\eta-\eta_2)\right] + C' \quad ...(23)$$

where, $A = \eta_1/(\eta_1-\eta_2)$, $B = \eta_2/(\eta_2-\eta_1)$ and C' is constant of integration.

To find the value of constant of integration C' choose an arbitrary point at the origin at the point of inflection in the shock-front transition region defined by the condition, $d^2\eta/dr^2 = 0$ we get,

$$d^2\eta/dr^2 = a_1 - c_1/\eta^2 = 0 \quad ...(24)$$

The solutions of the Eq. (24) which gives the point of inflection is

$$\eta'_{eq} = \pm\sqrt{c_1/a_1} \quad ...(25)$$

Using Eq. (25), the constant of integration C' we get

$$C' = -\left(g_1/a_1\right)\left[A\log\left(\eta'_{eq}-\eta_1\right) + B\log\left(\eta'_{eq}-\eta_1\right)\right] \quad ...(26)$$

Substituting the value C' of from Eq. (26) into Eq. (23), ultimately we get the exact solution for the particle velocity with respect to the distance as

$$r = (g_1/a_1)\left[A\log\left\{(\eta-\eta_1)/(\eta'_{eq}-\eta_1)\right\} + B\log\left\{(\eta-\eta_1)/(\eta'_{eq}-\eta_1)\right\}\right] \quad ...(27)$$

where, $A = \left\{\eta_1/(\eta_1-\eta_2)\right\}$, $B = \left\{\eta_2/(\eta_2-\eta_1)\right\}$

The exact solution for temperature and particle velocity of the gas, within the shock transition region, using the energy conservation Eq. (7) and Eq. (17) given as

$$T/T_0 = 1 + (\gamma-1)[\gamma M^2\eta^2/2 - \eta(1+\gamma M^2) + \left(1+\gamma M^2/2\right) + \chi] \quad ...(28)$$

where,

$$\chi = \left(\mu M\gamma^2/P_r\right)\left(a_1\eta^2 + b_1\eta + c_1/g_1\right)(\gamma/p_0\rho_0)^{1/2}$$

Eq. (28) gives the relation between temperature and the particle velocity. The obtained analytical expression shows the dependency of temperature on the particle velocity.

From Eq. (27) and Eq. (28), we can calculate temperature variations across the shock transition region with respect to the distance. In addition, on utilizing Eq. (4, 15, 20) into Eq. (16), we can easily determine the exact solution for the pressure variations across the shock transition region as

$$p/p_0 = \left[1 + \gamma M^2\left\{(2-\eta) + 3\gamma(\gamma-1)/4P_r\right\}\right] \quad ...(29)$$

Thus, Eq. (27) and Eq. (29) clearly show concurrently describe the dependence of the pressure across the shock-front on the distance. So, we can write a definite formula that illustrates the change-in-entropy across the shock of arbitrary strength in viscous heat-conducting fluid as

$$\left(\Delta S/R\right)_\eta = \gamma\left(\gamma-1\right)^{-1}\log\left(T/T_0\right) - \log\left(p/p_0\right) \quad ...(30)$$

The obtained expression for the change-in-entropy across the wave surface is obtained in terms of temperature and pressure gradient with adiabatic exponent respectively. Thus, ultimately the Eq. (30) demonstrates the entropy production across the shock-front for the gas is simply found by substituting Eq. (28) and Eq. (29) into Eq. (30).

Graphs have been plotted for all the flow variables such as particle velocity η, temperature T/T_0, pressure p/p_0, and change-in-entropy distribution $\Delta S/R$ in Figs. 1-4 within shock transition region.

3 Results and Discussion

This work put a forward discussion on a precise and exact solution for the internal structure of shock-front in a thermally heat-conducting viscous gaseous medium. The analytical expressions are obtained for

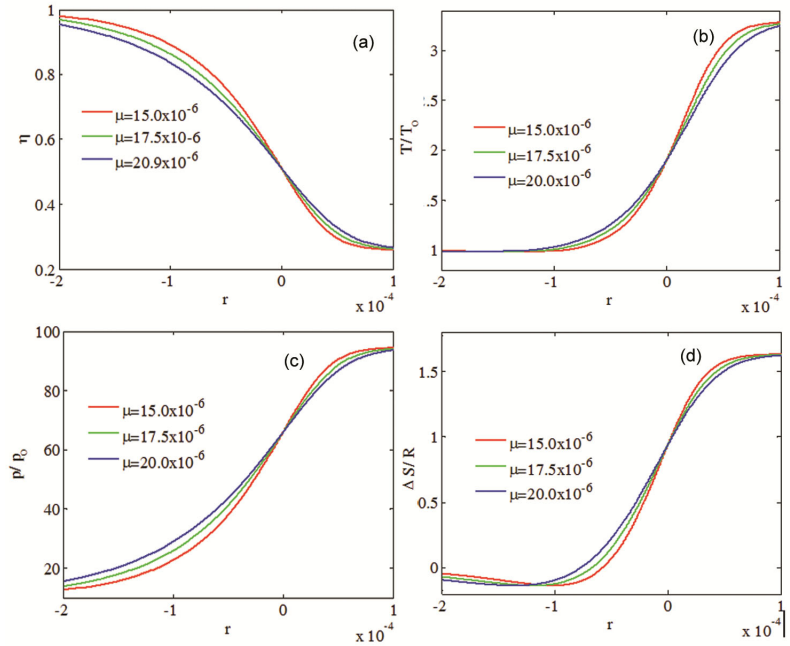

Fig. 1 — Variation of flow variables (a) particle velocity, (b) temperature, (c) pressure, and (d) change-in-entropy distribution within the shock transition region with distance r for various values of μ at M=3, $\gamma = 1.4$, Pr = 3/4, $p_0 = 0.9$ bar, and $\rho_0 = 1.20\ kg/m^3$.

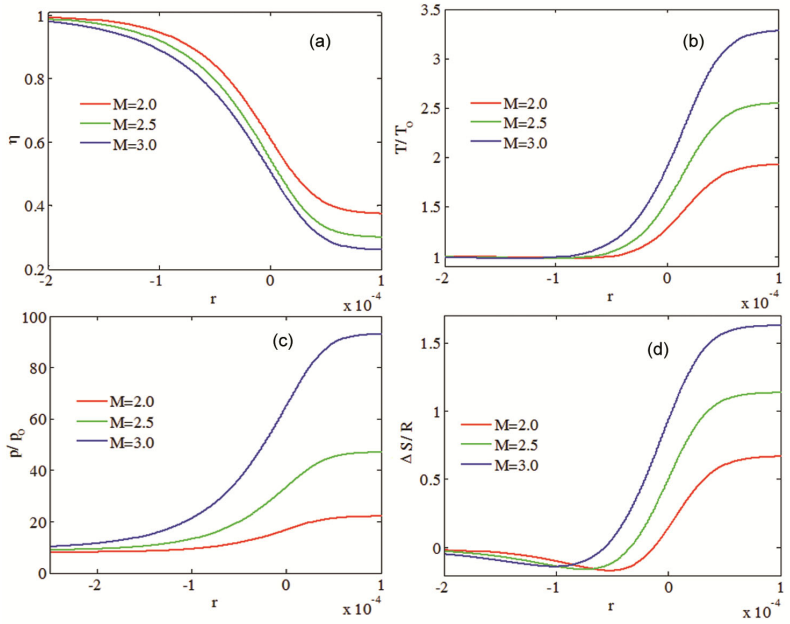

Fig. 2 — Variation of flow variables (a) particle velocity, (b) temperature,(c) pressure, and (d) change-in-entropy distribution within the shock transition region with distance r for various values of M at $\mu = 15.0 \times 10^{-6}$ Pa sec, $\gamma = 1.4$, Pr = 3/4, $p_0 = 0.9$ bar, and $\rho_0 = 1.20\ kg/m^3$.

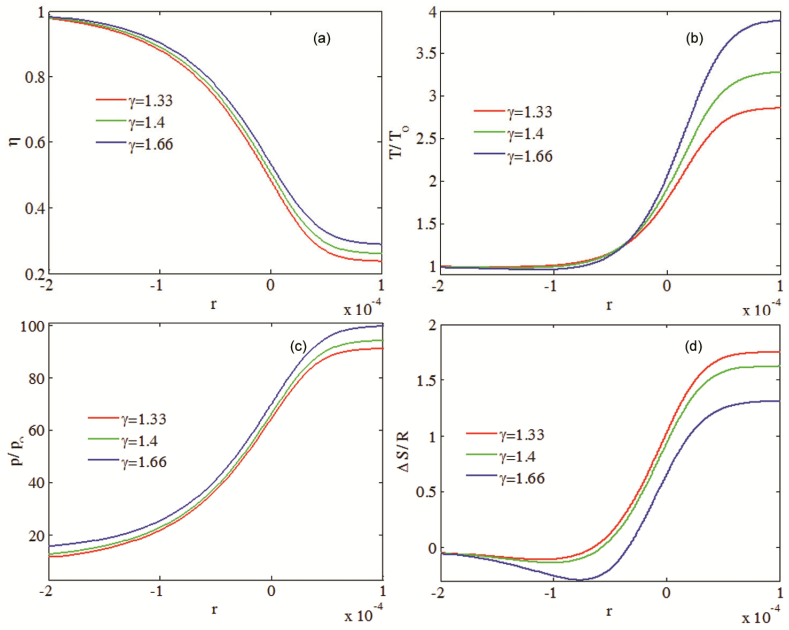

Fig. 3 — Variation of flow variables (a) particle velocity, (b) temperature, (c) pressure, and (d) change-in-entropy distribution within the shock transition region with distance r for various values of γ at *M*=3, $\mu = 15.0\times10^{-6}$ Pa sec, *Pr* = 3/4 , $p_0 = 0.9$ bar, and $\rho_0 = 1.20\ kg/m^3$.

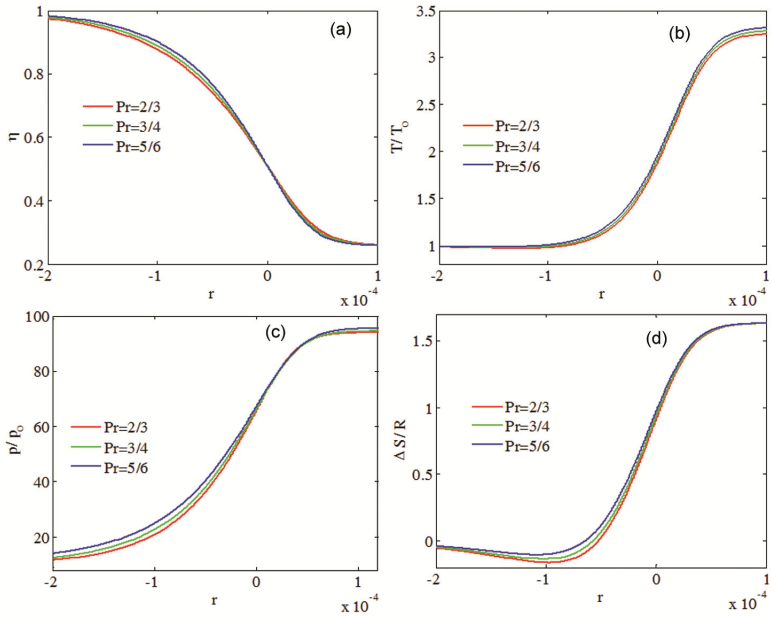

Fig. 4 — Variation of flow variables (a) particle velocity, (b) temperature, (c) pressure, and (d) change-in-entropy distribution within the shock transition region with distance r for various values of Prandtl number at *M*=3, $\mu = 15.0\times10^{-6}$ Pa sec, $\gamma = 1.4$, $p_0 = 0.9$ bar, and $\rho_0 = 1.20\ kg/m^3$.

the different flow variables such as the particle velocity η, temperature T/T_0, pressure p/p_0, and change-in-entropy $\Delta S/R$ with the variations in the physical flow parameters (μ, M, γ, P_r) given by Eq. (27-30), and discuss shock wave-front within the shock transition region. It is worth mentioning that while obtaining the

Table 1 — The thickness of shock-front in an ideal gas for $\gamma = 1.4$, $p_0 = 0.9$ bar and $\rho_0 = 1.20\ kg/m^3$ for various values of different parameters.

Mach Number M	Coefficient of viscosity μ [Pa sec]	Prandtl Number Pr	r_1(meter)	r_2(meter)	Thickness (r_2-r_1) (meter)
2.0		2/3	-0.0004764	0.0001855	0.0006619
	15.0×10^{-6}	3/4	-0.0004716	0.0001837	0.0006553
		5/6	-0.0004673	0.000182	0.0006493
		2/3	-0.0005558	0.0002165	0.0007723
	17.5×10^{-6}	3/4	-0.0005502	0.0002143	0.0007645
		5/6	-0.0005452	0.0002123	0.0007575
		2/3	-0.0006353	0.0002474	0.0008827
	20.0×10^{-6}	3/4	-0.0006288	0.0002449	0.0008737
		5/6	-0.000 6231	0.0002426	0.0008657
2.5		2/3	-0.0005511	0.0001735	0.0007246
	15.0×10^{-6}	3/4	-0.0005476	0.0001724	0.0007200
		5/6	-0.0005445	0.0001714	0.0007159
		2/3	-0.000643	0.0002024	0.0008454
	17.5×10^{-6}	3/4	-0.0006389	0.0002011	0.0008400
		5/6	-0.0006353	0.0002	0.0008353
		2/3	-0.0007348	0.0002313	0.0009661
	20.0×10^{-6}	3/4	-0.0007302	0.0002298	0.0009600
		5/6	-0.000 7261	0.0002285	0.0009546
3.0		2/3	-0.0007864	0.0001745	0.0009602
	15.0×10^{-6}	3/4	-0.000783	0.0001737	0.0009567
		5/6	-0.0007799	0.0001731	0.0009530
		2/3	-0.0009174	0.0002036	0.001121
	17.5×10^{-6}	3/4	-0.0009135	0.0002027	0.0011162
		5/6	-0.0009099	0.0002019	0.0011118
		2/3	-0.00 1049	0.0002327	0.0012817
	20.0×10^{-6}	3/4	-0.001044	0.0002317	0.0012757
		5/6	-0.00104	0.0002308	0.0012708

analytical expressions of flow variables, other disturbances such as reflections, oblique waves, overlapping waves, distorted waves, and wave interactions *etc*., in it, but we go by neglecting the disturbance caused by it. The expressions for the particle velocity, temperature, pressure, and change-in-entropy distribution are the functions of the wave-front distance *r*, the Prandtl number, the coefficient of viscosity μ, the strength of shock *M*, and the adiabatic index γ of the gas. Therefore, we have taken the values of the constant parameters are $\mu = \{15, 17.5, 20\}$ (in units of 10^{-6} Pa sec), *Pr* = {2/3, 3/4, 5/6}, *M* = {2.0, 2.5, 3.0}, $\gamma = \{1.33, 1.4, 1.66\}$, initial pressure $p_0 = 0.9$ bar and initial density $\rho_0 = 1.20\ kg/m^3$. MATLAB code are used to make numerical computations and for graphs.

We have made the following observations from the Table 1 as:

(i). On increasing the value of shock strength *M*, keeping μ constant, the thickness of shock-front increases. Similar observations are obtained for each value of μ.

(ii). The thickness of the shock-front increases with increasing μ, keeping fixed value of *M*. we also notice that it follows the similar observation obtains for each value of *M*.

(iii). The thickness of the shock wave-front decreases with increasing Prandtl number, at a constant value of *M* and μ .In addition, we also observe from the table that it gives the same observations for each value of *M* and μ .

Thus, from the obtained interpretations, it can be concluded that in a heat conducting medium with viscosity have a dominant effect on the thickness of the shock-fronts.

The expressions for the variation of the flow variables given in Eq. (27-30) within the shock

transition region with distance r for different values of μ at a fixed value of M=3, $\gamma = 1.4$, $p_0 = 0.9$ bar, $\rho_0 = 1.20\ kg/m^3$, Pr = 3/4 are shown in Fig. 1. It is observed from the Fig. 1, the spreading of the flow variables around the point of inflection increases with increasing the value of μ, in both the regions of stream. We also notice that analogous distribution of pattern are observed for all the flow variables (η, T/T_0, p/p_0 , $\Delta s/R_i$) for each values of μ .Thus, the thickness of shock-front increases with increasing μ .

The expression for the variations in the flow variables within shock transition region with distance r for different values of M=2.0, 2.5, 3.0 at a fixed value of $\mu = 15.0\times10^{-6}$ Pa sec, $\gamma = 1.4$, $p_0 = 0.9$ bar, ρ_0=1.20 kg/m^3 and Pr = 3/4 are shown in Fig. 2. It is observed that the spreading of the flow variables such as the particle velocity, temperature, and the change-in-entropy distribution are more distinguishable towards the upstream side, whereas, these plots are indistinguishable towards the downstream side. The pressure variation in both sides *i.e.*, ahead and behind at the point of inflection are distinguishable. This figure shows that the spreading for all the flow variables such as the particle velocity, temperature, pressure, and change-in-entropy distribution increases with increasing M. Thus, the shock-front thickness increases with increasing shock strength. Here, from the above results it can be seen that, for a small value of M, the observation is similar to that obtained in the absence of heat conduction[35].

Figure 3 depicts the variation of the particle velocity, temperature, pressure, and change-in-entropy distribution within the shock transition region with distance r for various values of adiabatic exponent at fixed values of M = 3, $\mu = 15.0\times10^{-6}$ Pa sec, $p_0 = 0.9$ bar, ρ_0=1.20 kg/m^3 and Pr = 3/4.

From Fig. 3 apparent that the plots for all the flow variables are distinguishable towards the upstream side but not so much distinguishable towards the downstream side. We also notice that for $\gamma = 1.33$, the spreading of the particle velocity, temperature, and pressure is small, and it increases with increasing value of γ . In the case of the change-in-entropy distribution, the spreading is large at $\gamma = 1.33$, and it decreases with increasing γ . Fig. 3 shows that under consideration of the viscosity with heat conducting medium, the thickness of shock-front is increases with increasing adiabatic index. Noticeably, the behavior and nature of graphs of shock-front thickness is similar to variation obtained by Anand & Yadav[35] for lower shock strength.

Figure 4 shows the variation of the particle velocity, temperature, pressure, and change-in-entropy distribution within the shock transition region with distance r for various values of Prandtl number for the values of physical flow parameters, M=3, $\gamma = 1.4$, $\mu = 15.0\times10^{-6}$ Pa sec, $p_0 = 0.9$ bar and $\rho_0 = 1.20\ kg/m^3$.

In Fig. 4, it can be observed that the variations of the flow variables are indistinguishable in upstream and downstream sides around the point of inflection except in the case of pressure distribution show distinguishable towards ahead and behind of the point of inflection.

It is noticeable that the spreading of the flow variable is large at Pr=2/3 and decreases with increasing Pr. Thus, the thickness of flow variables decreases with increasing Prandtl number. It is momentous to mention that Hamad[17, 18] also solved a similar problem using different technique and our results, confirm their findings.

3.1 Comparative study for the structure of shock-front

The shock-front thickness (Δr) of the shock wave is defined[9, 13, 24] by

$$\Delta r = (U - u_0) \Big/ \left(du/dr\right)_{\max} \qquad ...(31)$$

where, $\Delta r = r_2 - r_1$ is the shock-front thickness of the shock-front between two bounded states. It is also known as Prandtl front thickness. Since, for a stationary shock-front, geometrically the flow gradients are large when considering viscous and heat conducting terms. For measurement of thickness due to large gradients, the effective shock-front thickness[22] is defined as

$$\frac{u_0 - U}{\Delta r} = \left|\frac{du}{dr}\right|_{\max} \qquad ...(32)$$

Thus, to obtain the non-dimensional terms of the effective shock-front thickness in terms of the mean-free path λ_0 is given by

Table 2 — Inverse shock-front thickness (Λ) for various values of *Pr*=3/4, *M*=1.2, $p_0 = 0.9$ bar, $\mu = 15.0 \times 10^{-6}$ Pa sec, $\rho_0 = 1.20\ kg/m^3$.

Prandtl Number (*Pr*)	Adiabatic index γ	Inverse shock-front thickness (Λ)	
		Present Study	Khapra's Study
0	1.33	0.014805	-
	1.4	0.014774	0.0016975
	1.66	0.014230	0.0005179
2/3	1.33	0.016995	-
	1.4	0.018339	0.052828
	1.66	0.022965	0.041522
3/4	1.33	0.017386	-
	1.4	0.018909	0.054014
	1.66	0.024876	0.042437
∞	1.33	0.000006	-
	1.4	0.000005	0.065741
	1.66	0.000002	0.054009

Table 3 — Inverse shock-front thickness (Λ) at various values of Mach number and adiabatic index at constant values of *Pr*=3/4, $p_0 = 0.9$ bar, $\mu = 15.0 \times 10^{-6}$ Pa sec, $\rho_0 = 1.20\ kg/m^3$.

Adiabatic index γ	*M* = 1.1		*M* = 1.5		*M* = 2.0	
	Present Study	Khapra's Study	Present Study	Khapra's Study	Present Study	Khapra's Study
1.33	0.010501	-	0.022979	-	0.026044	-
1.4	0.012221	0.803340	0.025101	0.40689	0.027598	0.22231
1.66	0.018383	0.792484	0.029789	0.39071	0.031589	0.21086

$$\theta = \Delta r / \lambda_0 \qquad ...(33)$$

where, $\lambda_0 = \mu\sqrt{\pi/2\rho_0 p_0}$

In terms of scaled distance[34], the Inverse shock-front thickness (Λ) is defined in terms of mean free path of the shock-front thickness is given by

$$\Lambda = \lambda_0 / \Delta r \qquad ...(34)$$

From Table 2, the effect of variation in the structure of inverse shock-front thickness for various value of Prandtl number and adiabatic index of the gas at a constant value of physical flow parameters can be summarized in the following ways:

(a). For a fixed value of adiabatic index, the inverse shock-front thickness increases with increasing Prandtl number. Our results is similar to that the results obtained by Khapra *et al*[33].

(b). The inverse shock-front thickness increases with increase in the adiabatic index but at the lower $(\Pr \to 0)$ and higher $(\Pr \to \infty)$ value of Prandtl number, the inverse shock thickness decreases, and gets closer observations as presented in the literature[33].

From the Table 3, it can be summarized that:

On increasing adiabatic index γ , while keeping *M* fixed, the inverse shock thickness increases, and analogous results are obtained for different values of *M*. On the other hand, as γ increases, the inverse shock thickness decreases, which is in contrast to Khapra's results. This may be attributed to the fact that, at lower shock strength, the heat conduction[36] terms become negligible. Therefore, we are getting different order of thickness and trends of flow variables with flow parameters. In the case of at higher range of shock strength $M > 2$, the inverse shock-front thickness decreases with increasing γ , similar to the result of Khapra *et al*[33]. Thus, from, above observations, it is found that the results obtained by different methods give almost the same outcome in qualitatively.

4 Conclusions

In this work, we have made an attempt to understand the formation and structure of a steady shock-front in a viscous and heat conductive gaseous phase medium. The exact solutions for the different flow variables $(\eta, T/T_0, p/p_0, \Delta s/R_i)$ are derived

within the shock transition region. In addition, the thickness and inverse shock-front thickness with various flow parameters have been explored, and analysing the effects on the flow variables such as pressure, temperature, entropy, *etc*. within the transition region between the shock-front. On comparison of obtained results with the results present in the literature, we see that the present finding show good agreement in both the aspects qualitatively and quantitatively. Such a problem is of great attention not only in space science but also highly relevant to the problem of the origin and understanding of the shock waves. Our results show that the structure of shock waves in a medium is greatly affected by both the viscosity and heat conduction properties of the medium.

Based on the non-dimensional analysis of a continuous, viscous, and heat-conducting fluid medium, the following conclusions can be stated as follows:

1 On increasing the value of the coefficient of viscosity and Mach number, the shock wave-front thickness increases. (Table 1, Figs.1, 2)
2 The thickness of the shock-front decreases with increasing the adiabatic index.(Table1, Fig. 3)
3 The thickness of the shock-front decreases with increasing the Prandtl number.(Table 1, Fig. 4)
4 On increasing the value of Prandtl number, the inverse shock-front thickness increases. (Table 2)
5 On increasing adiabatic index, the inverse shock-front thickness increases, and similar results are obtained for different Mach number. (see Table 3)

It is proposed to extend the scope of this work to non-ideal fluids, such as water, air, blood, *etc*. This will help to better understanding the internal structure of shockwaves and distribution of the flow variables such as pressure, temperature, entropy production, *etc*., within the shock transition region.

Acknowledgment

One of the authors Anmol Singh would like to thanks to UGC New Delhi, Government of India, for financial assistance.

References

1 Zapryagaev V, Kiselev N & Gubanov D, *Aerospace*, 5 (2018) 60.
2 Ligrani P M, McNabb E S, Collopy H, Anderson M & Marko SM, *Adv Aerodyn*, 2 (2020) 1.
3 Rankine W J M, *Philos Trans R Soc*, 160 (1870) 277.
4 Hugoniot P H, *J Ecole Polytech*, 58 (1889) 1.
5 Taylor G I, *R Soc Lond A*, 84 (1910) 371.
6 Becker R, *Z Phys*, 8 (1929) 321.
7 Thomas L H, *J Chem Phys*, 12 (1944) 449.
8 Wang C C S, *Dept Eng Res Rep*, Univ Michigan UMH-3-F (APL/JHU CM-503), 1948.
9 Libby P A & Morduchow M, *J Aeronaut Sci*, 16 (1949) 674.
10 Meyerhoff L, *J Aeronaut Sci*, 17 (1950) 775.
11 Puckett A E & Stewart H J, *Q Appl Math*, 7 (1950) 457.
12 Gilbarg D & Paolucci D T, *J Rat Mech Anal*, 2 (1953) 617.
13 Von Mises R, *J Aeronaut Sci*, 17 (1950) 551.
14 Landau L D & Lifshitz E M, Fluid Mechanics Course of Theoretical Physics (Pergamon Press, Oxford), 1987.
15 Hicks B L, Yen S M & Reilly B J, *J Fluid Mech*, 53 (1970) 85.
16 ChapmanS & Cowling T, The Mathematical theory of non-uniform gases (Cambridge University Press, Cambridge), 1970.
17 Hamad H, *Proc R Soc Lond A*, 452 (1996) 2163.
18 Hamad H, *Acta Mechanica*, 140 (2000) 65.
19 Iannelli J, *J Comput Phys*, 230 (2011) 260.
20 Myong R S, *AIAA J*, 52 (2014) 1075.
21 Elizarova T G, Shirokov I A & Montero S, *AIP Conf Proc*, 762 (2005) 1253.
22 Zel'dovichYa B & Raizer Y P, Physics of Shock Waves and High Temperature Hydrodynamic Phenomena, (Academic Press, New York), 1966.
23 Uribe F J & Velasco R M, *Phys Rev E*, 97 (2018) 1.
24 Reddy M H L & Dadzie S K, *Shock Waves*, 30 (2020) 513.
25 Shoev G V, Timokhin M Y & Bondar Y A, *Phys Fluids*, 32 (2020) 041703.
26 Ohr Y G, *Phys Fluids*, 32 (2020) 061707.
27 Margolin L G, Plesko C S & Reisner J M, *Physica D: Non-Linear Phenomena*, 403 (2020)132308.
28 Jiang Z, Zhao W, Chen W & Agarwal R K, *Shock Waves*, 29 (2019)1227.
29 Wibisono I, Yanuar, Kosasih E A & Alief M, *AIP Conf Proc*, 2062 (2019) 020004.
30 Khidr M A & Mahmoud M A A, *Astrophys Space Sci*, 113 (1985) 289.
31 Johnson B M, *J Fluid Mech*, 726 (2013) 1.
32 Patel A & Singh M, *Shock Waves*, 29 (2019) 427.
33 Khapra D & Patel A, *Shock Waves*, 30 (2020) 585.
34 Anand R K & Yadav H C, *Phys Scr*, 83 (2011) 065402.
35 Anand R K & Yadav H C, *Acta Phy Pol A*, 129 (2016) 28.
36 Berezin Y A & Dudnikova G I, *J Appl Mech Tech Phys*, 13 (1972) 139.
37 Thompson P A, Strock T W & Lim D S, *Phys Fluids*, 26 (1983) 48.